Journal Pre-proof

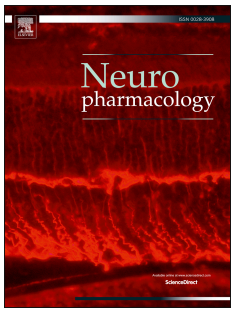

NLRP3 inflammasome inhibition with MCC950 improves insulin sensitivity and inflammation in a mouse model of frontotemporal dementia

Claire Hull, Ruta Dekeryte, Heather Buchanan, Sarah Kamli-Salino, Avril Robertson, Mirela Delibegovic, Bettina Platt

PII: S0028-3908(20)30373-7

DOI: https://doi.org/10.1016/j.neuropharm.2020.108305

Reference: NP 108305

To appear in: *Neuropharmacology*

Received Date: 15 April 2020

Revised Date: 13 August 2020

Accepted Date: 8 September 2020

Please cite this article as: Hull, C., Dekeryte, R., Buchanan, H., Kamli-Salino, S., Robertson, A., Delibegovic, M., Platt, B., NLRP3 inflammasome inhibition with MCC950 improves insulin sensitivity and inflammation in a mouse model of frontotemporal dementia, *Neuropharmacology* (2020), doi: https://doi.org/10.1016/j.neuropharm.2020.108305.

CRediT Statement of Contributions

BP and MD conceptualised, designed and planned the experiments, within input from AR, who also provided the compound and experimental guidance and PK data for the treatment regime. The majority of experiments and related data analyses were conducted by CH, with additional experimental contributions from RD, HB, and SKS. The experimenters conducted their own individual data analysis, with CH and BP overseeing the finalisation of statistical procedures. The manuscript was initially written by CH and BP with contributions from all co-authors. All authors have read, edited and approved the manuscript. Financial support for the project was provided by BP and MD.

NLRP3 inflammasome inhibition with MCC950 improves insulin sensitivity and inflammation in a mouse model of frontotemporal dementia

Claire Hull[1], Ruta Dekeryte[1], Heather Buchanan[1], Sarah Kamli-Salino[1], Avril Robertson[2], Mirela Delibegovic[1] and Bettina Platt*[1]

[1] Institute of Medical Sciences, School of Medicine,

Medical Sciences & Nutrition, Foresterhill,

University of Aberdeen, Aberdeen AB25 2ZD, Scotland, UK

[2] School of Chemistry and Molecular Bioscience, The University of Queensland,

St Lucia, QLD, 4072, Australia

***Correspondence to:**

Prof. Bettina Platt, PhD, FSB
Chair in Translational Neuroscience
School of Medicine, Medical Sciences & Nutrition
University of Aberdeen
Foresterhill
ABERDEEN AB25 2ZD
Scotland, UK
Tel.: (+44) 1224 437402
FAX: (+44) 1224 437465
Email: b.platt@abdn.ac.uk

1.1 Abstract

The NOD-like receptor pyrin domain-containing protein 3 (NLRP3) inflammasome has been implicated as a crucial component in both neurodegeneration and diabetes. However, the role of metabolic signalling pathways and the NLRP3 inflammasome in frontotemporal dementia remain largely elusive. We therefore investigated the effects of an NLRP3 inhibitor (MCC950) in a murine tau knock-in ($PLB2_{TAU}$) model vs. wild-type (PLB_{WT}) control mice. In male $PLB2_{TAU}$ mice (4 months at start of study), MCC950 treatment (20 mg/kg, for 12 weeks) improved insulin sensitivity and reduced circulating plasma insulin levels. Further molecular analysis suggested normalisation in insulin signalling pathways in both liver and muscle tissue. Treatment also resulted in improvements in inflammation and ER stress signalling, both peripherally and centrally, alongside a partial normalisation of phospho-tau levels.

Overall, we provide evidence that MCC950 improved metabolic, inflammatory and frontotemporal dementia (FTD) relevant phenotypes in multiple tissues. NLRP3 inhibition may therefore offer a therapeutic approach to ameliorate FTD pathology.

Keywords: transgenic, knock-in, diabetes, insulin, dementia, NLRP3, inflammasome, ER stress, UPR, Inflammation.

1.2 Introduction

Dementia and type 2 diabetes mellitus (T2D) are two of the most prevalent conditions in the elderly. To date, there is increasing evidence supporting a link between metabolic dysfunction and neurodegenerative diseases such as Alzheimer's disease (AD) and potentially also frontotemporal dementia (FTD) (Hull et al., 2019; Lauretti et al., 2017; Marciniak et al., 2017; Yarchoan et al., 2014). Inflammation, hyperglycaemia, insulin resistance and glucose intolerance have all been shown to contribute to the pathological process of both T2D and dementia, suggesting possible shared molecular and cellular pathways (Bello-Chavolla et al., 2019; Mushtaq et al., 2015; Strachan et al., 2008). However, the precise mechanisms underlying this association remain unknown, especially with regards to tauopathies.

Metabolic research in FTD/FTLD lacks behind the extensive work conducted in AD; larger epidemiological studies are still missing. Some reports identified elevated insulin levels, triglycerides and changes in glucose metabolism in FTD patients, but these studies are so far based on small cohorts only. Importantly, a recent study (Liou et al., 2019) concluded that dysregulated insulin signaling in degenerating brain regions mediate brain metabolic dysfunction and contribute to disease pathogenesis in FTD, akin to other types of dementia.

The central nervous system (CNS) is recognised to have a continuous interplay with the innate and the adaptive immune systems, where resident microglia and immune cells play important roles. The innate immune system is activated through pattern recognition receptors such as the nucleotide-binding oligomerisation domain (NOD)-like receptors (NLRs). Activation of NLRs enables the formation and activation of inflammasome complexes (Broz and Dixit, 2016; Latz et al., 2013). Inflammasome activation is a crucial

signalling pathway in the maturation of two proinflammatory cytokines (interleukin 1β (IL-1β) and IL-18) through cleavage of caspase-1 (Broz and Dixit, 2016; Latz et al., 2013). The NLRP3 inflammasome is the most extensively studied inflammasome and has been implicated as a central component in the development of diabetes and neurodegenerative diseases (Ising et al., 2019; Jiang et al., 2018; Rheinheimer et al., 2017). Neuroinflammatory pathways rely on the activation of the inflammasome and are crucial in neurodegeneration, with extensive evidence indicating that both IL-18 and IL-1β contribute to pathogenesis (Halle et al., 2008; Tan et al., 2013). Importantly, it has recently been demonstrated that activation of the NLRP3 inflammasome may drive tau pathology through regulation of tau kinases and phosphatases in FTD (Ising et al., 2019). The authors revealed that loss of NLRP3 function reduced tau hyperphosphorylation and rescued spatial memory deficits present in a mouse model (Tau22). Further links between NLRP3 activation and neurodegeneration were indicated by the secretion of IL-1β through activation of the inflammasome by pathological tau (Španić et al., 2019; Stancu et al., 2019). In addition, inhibition of the NLRP3 inflammasome was reported to decrease amyloid-beta (Aβ) levels in APP/PS1 mouse model (Heneka et al., 2013) and improve cognition in 3xTgAD mice (Daniels et al., 2016). Elevated levels of NLRP3 have also been observed in diabetic patients (Jiang et al., 2018; Lee et al., 2013), and mice deficient in caspase-1 and NLRP3 were resistant to the high-fat diet-induced obesity and protected from obesity-induced insulin resistance (Stienstra et al., 2011). Moreover, exercise-mediated weight loss and caloric restriction significantly lowered expression levels of NLRP3 in adipose tissue, as well as improving sensitivity to insulin (Vandanmagsar et al., 2011). Collectively, this research suggests that targeting the NLRP3 inflammasome may be an innovative therapeutic approach to target both neuronal inflammation and metabolic deficits in neurodegenerative disorders.

MCC950 (also known as CRID3, CP-456,773 and CAS 210826-40-7) is currently the most potent and selective small molecule inhibitor of the NLRP3 inflammasome. It binds to NLRP3 and blocks NLRP3 ATPase activity, subsequently inhibiting inflammasome formation and activation (Coll et al., 2019; Tapia-Abellán et al., 2019). The pharmacokinetics of this compounds have been independently confirmed (Coll et al., 2015; Primiano et al., 2016), and it has been reported to display neuroprotective benefits in multiple disorders, including neurodegenerative diseases and diabetes (Dempsey et al., 2017; Fan et al., 2018; Fekete et al., 2019; Qi et al., 2018; Ward et al., 2019; Zhai et al., 2018). MCC950 reduced the accumulation Aβ and improved cognitive function in APP/PS1 mice, this was attributed to the inhibition of NLRP3 inflammasome activation and the reduction of Aβ accumulation through increased clearance (Dempsey et al., 2017). In agreement with this study, it was also reported that MCC950 reduced microglia reactivity, and memory impairments, and restored expression of inhibitory neuronal ligands in another AD model (APPNL-F/NL-F)(Fekete et al., 2019). Additionally, MCC950 significantly improved insulin sensitivity in db/db mice, a common model of insulin resistance, as well as reducing depression and anxiety-like behaviours and improving cognitive function (Zhai et al., 2018).

Here, we investigated the effect of MCC950 in a novel murine knock-in model of FTD, $PLB2_{TAU}$ (Hull et al., 2019; Koss et al., 2016). These mice express a single copy of mutated hTau (2N4R TauP301L + R406W), which yields brain phospho-Tau pathology for an FTD-like phenotype as well as changes in insulin sensitivity, glucose homeostasis and inflammatory related markers (Hull et al., 2019). We provide evidence that MCC950 improved insulin sensitivity, reduced circulating plasma insulin levels, and resulted in changes in ER stress signalling and insulin signalling, both peripherally and centrally.

2. Materials & Methods

2.1 Animals

Four month old male PLB_{WT} (n=23) and $PLB2_{TAU}$ (n=22) mice were generated as previously described (Koss et al., 2016). Of note, the PLB_{WT} mice, which serve as controls for all PLB

lines, were originally created as littermates from the parental $PLB1_{Double}$ mice. All mice were maintained at Charles River UK on a C57BL6 background, and all lines are regularly crossed with unrelated C57BL6/J wildtype mice (Elite breeders from Charles River). All mice were housed and tested in accordance with UK Home Office, the EU directive 63/2010E and the Animal (Scientific Procedures) Act 1986. Mice were delivered to our facility at least 1 week before testing. Animals were housed in a climate–controlled holding room (20–21°C, 60–65%, relative humidity) with ad libitum access to water and food with a 12-hour day/night cycle (lights on at 7am).

2.2 MCC950 Treatment

PLB_{WT} and $PLB2_{TAU}$ were randomised and counterbalanced using a random number generator (www.random.org), into 2 experimental groups: PLB_{WT} Vehicle (n=13), PLB_{WT} MCC950 (n=10), $PLB2_{TAU}$ Vehicle (n=11) and $PLB2_{TAU}$ MCC950 (n=11). The experimenter was not blinded with regards to genotype and treatment conditions due to the requirement to immediately identify adverse effects of treatment. Vehicle (PBS) or MCC950 (20mg/kg in PBS, Coll et al., 2019) was administered by i.p injection once daily, five times a week for a total of 12 weeks (see supplementary figure 1). MCC950 once dissolved in PBS was stored at 4 ^{o}C for no longer than a week. *In vivo* experiments were performed two weeks prior to treatment (baseline / pre-treatment), and during the last 7 weeks of the study.

2.3 *In Vivo* characterisation

2.3.1 Glucose, insulin, pyruvate tolerance tests & EchoMRI

Glucose (GTT), insulin (ITT) and pyruvate (PTT) tolerance tests were carried out as described previously (Hull et al., 2019). Briefly, tail blood glucose was determined using an AlphaTRAK glucometer (Berkshire, UK). GTTs and ITTs were performed in 5 hour fasted mice, and PTTs

were performed in overnight fasted mice. Fasting blood glucose (time 0) were recorded, followed by i.p. injection of glucose, insulin or pyruvate: GTT: 2 mg/g body weight dose of glucose (20% w/v glucose), ITT: 0.75 IU/g body weight dose of human insulin (Humulin R; Eli Lilly), PTT: 2mg/g body weight dose of pyruvate (20% w/v pyruvate). Blood glucose levels were determined at 15, 30, 60 and 90 minutes post-injection. EchoMRI (EchoMRI, Houston, TX, USA) was used to assess body composition (adiposity and lean body mass) (Robinson et al., 2013).

2.3.2 PhenoTyper home cage and RotaRod

The PhenoTyper homecage observation system (Noldus, The Netherlands; Robinson et al., 2013) was used to assess locomotor and circadian activity. Activity was recorded for 7 consecutive days and data extracted in 1 hour or 10-minute time bins. The first 3 hours of recording served as habituation to a new environment. The mean hourly activity was calculated over 24 hours. The animals had *ad libitum* access to a weighted amount of water and food and the amount consumed was recorded. The RotaRod test was carried out as described previously (Hull et al., 2019). Briefly, automated four lane accelerating RotaRods (UgoBasile NG Rotarod 1.3.2R) were used to study motor learning and motor coordination. Testing occurred on 2 consecutive days with 4 trials per day (5-minute intervals) using an acceleration from 1-45 rpm over 300 seconds.

2.4 Insulin ELISA

Blood serum samples from 5 hour fasted mice were used to quantify insulin levels using an insulin ELISA (Merck Millipore, Cat No: EZRMI-13K). This assay was carried out following manufacturers' instructions and absorbance measured at 450 nm and 590 nm using a BMG Labtech FLUOstar Omega plate reader (BMG Labtech, Germany).

2.5 Ex vivo molecular characterisation

2.5.1 Blood plasma collection

20 µl of blood was collected from the tail of 5-hour fast mice into a BD Microtainer SST Tube (BD Biosciences, CA, USA). Blood tubes were left to coagulate at room temperature (RT) for 30 minutes and centrifuged at 7500 g for 15 minutes at 4 ^{o}C. Serum was aliquoted and stored at -80^{o}C.

2.5.2 Brain, muscle and liver tissue

All mice were fasted for 5 hours and an i.p. injection of insulin (10 mU/g body weight) was administered. Mice were sacrificed by neck dislocation; liver, muscle and brain tissue snap-frozen in liquid nitrogen and stored at -80 ^{o}C. Tissue was prepared as previously described (Hull et al., 2019). In short, muscle or liver tissue were homogenized in RIPA lysis buffer (10 mM Tris-HCl, 150mM sodium chloride (NaCl), 0.1% SDS, 1% triton, 1% sodium deoxycholate, 5 mM ethylenediaminetetraacetic acid (EDTA), 1 mM sodium fluoride (NaF), 1 mM sodium orthovanadate (Na_3VO_4): pH=7.4). Brain tissue (whole brain) was homogenized in NP40 lysis buffer (1 M HEPES, 5 M NaCl, 0.1 M EDTA 1%, NP-40 (Sigma, Dorset, UK): pH = 7.6). Both NP40 and RIPA buffer were supplemented with PhosSTOP (Roche) and complete protease inhibitor (Roche) tablets (1 tablet / 10 ml). Homogenates were centrifuged (14,000g, 4 ^{o}C, 20 min) and supernatant collected and stored at −80 °C. For detection of tau, heat stable fractions were isolated by further heating the supernatant from brain tissue at 90 °C for 10 minutes before further centrifugation (14,000g, 4 ^{o}C, and 10 min) and the resulting supernatant collected.

2.5.3 Protein analyses

Protein analyses were carried out as described by Hull et al (Hull et al., 2019). In brief, using a BCA protein assay (Sigma, Dorset, UK) sample protein concentration was adjusted to a final concentration of 3 µg/µl. Samples were prepared with lithium dodecyl sulphate (LDS, ThermoFisher Scientific, Paisley, UK), 15 mM dithiothreitol (DTT; Sigma) and NP40 or RIPA lysis buffer. Samples were heated for 10 minutes at 70 ^{o}C and separated on a pre-cast NuPage 4-12% sodium Bis-Tris electrophoresis gels. Electrophoresis was conducted for 45 minutes at 200 V in MOPS buffer and transferred onto a nitrocellulose (0.45 µm pore size, Invitrogen, UK) membrane (NuPage transfer buffer in dH2O with 10% methanol) at 25V for 1 hour. Tris-buffered saline with Tween (TBST) (0.05% Tween, 50 mM Trizma base, 150 mM NaCl) was used for washing (3 x 15 minutes). After transfer, membranes were blocked (5% milk powder in TBST) for 1 hour at RT. Subsequently, membranes were washed in TBST (3x10 mins) and incubated overnight at 4 ^{o}C in primary antibodies. Primary antibodies (Suppl. Table 1) were prepared using 5% BSA, 0.05% sodium azide and TBST. The following day membranes were washed and incubated in appropriate secondary antibodies (Suppl. Table 1). Western blots were visualised using freshly prepared enhanced chemiluminescent substrate (ECL; 0.015% hydrogen peroxide (H_2O_2), 30 µM coumeric acid in 1.25 mM luminol). Images were captured using a Vilber-Fusion chemiluminescence-imaging camera and Fusion Software (PEQLAB).

2.5.4 Quantification

Coomassie Blue was used as a protein loading control for Western blots as previously published (Plucinska et al., 2014). Densitometric analysis of 16-bit Western blots images was performed using ImageJ (NIH) software. Data for phospho-markers were first normalised to

total protein levels prior to expression relative to PLB_{WT} controls; all other markers were normalised to total protein and expressed relative to PLB_{WT} controls.

2.5.5 Quantitative polymerase chain reaction (qPCR)

Quantitative PCR was carried out as described previously (Hull et al., 2019). Briefly, total RNA was isolated from liver and cortical mouse tissue using TRIReagent (Ambion, Warrington, UK) according to the manufacturer's protocol. 1 µg of total RNA were used to synthesize cDNA using the bioline cDNA synthesis kit (Bioline, London, UK). Target genes were amplified using GoTaq qPCR Master Mix (Promega, Southampton, UK), in a Roche LightCycler® 480 System (Roche diagnostics, Burgess Hill, UK). The geometric mean of three of the most stable reference genes were used to normalise data. Gene expression was calculated using the comparative Ct method ($2^{-\delta\delta Ct}$). A list of primer sequences for qPCR are listed in Suppl. Table 2.

2.6 Statistical analysis

Statistical analysis was performed using Prism (V6, Graph-Pad). Nonlinear regression analysis with one-phase decay was used for habituation data (Robinson et al., 2013). Statistical analysis was preformed using a Shapiro-Wilk normality test to confirm a normal distribution, followed by a two-way ANOVA with Bonferroni post-hoc tests or two-tailed Student's t-tests, where appropriate (i.e. paired comparison). For all data, $p<0.05$ was considered reliable.

3. Results

3.1 Body weights and metabolic phenotype

Body weights, glucose, insulin and pyruvate intolerance were examined over the 12-week MCC950 treatment study in 8-month old male $PLB2_{TAU}$ mice and their age-matched PLB_{WT} controls. $PLB2_{TAU}$ mice had lower body weights compared to WT controls (-12%, Fig 1a) (Hull et al., 2019), MCC950 did not affect body weight (Fig. 1a, b) or body adiposity (Fig. 1c) as indicated by EchoMRI data. We next assessed metabolic control in $PLB2_{TAU}$ mice, (Hull et al., 2019), and found $PLB2_{TAU}$ mice to be glucose intolerant and insulin resistant (Fig. 1d, f, h). Furthermore, following MCC950 treatment no improvement in glucose or pyruvate tolerance was detected in either PLB_{WT} and $PLB2_{TAU}$ mice at 8 month of age (Fig. 1d-e, h-i). Interestingly, ITT tests revealed that both PLB_{WT} ($p<0.01$, $F(1, 84) = 10.09$, Fig. 1f) and $PLB2_{TAU}$ mice ($p<0.01$, $F(1, 82) = 9.878$) displayed an overall drug effect following treatment. However, PLB_{WT} mice presented with a slight resistance to insulin following MCC950 treatment, reaching significance at the 60-minute time point ($p<0.05$). In contrast, $PLB2_{TAU}$ mice exhibited a slight improvement in insulin tolerance compared to vehicle treated $PLB2_{TAU}$ mice, with the 30-minute time point reaching significance ($p<0.05$). Analysis of total glycaemic excursion revealed a significant increase in area under the curve following MCC950 treatment in PLB_{WT} mice (+38%, $p<0.05$, Fig. 1g). $PLB2_{TAU}$ mice presented with an overall genotype effect ($p<0.01$, $F(1, 38) = 8.816$), with a significant reduction in overall glucose production following MCC950 treatment (-26%, $p<0.01$, Fig. 1e). $PLB2_{TAU}$ mice have elevated basal insulin levels compared to age-matched controls (Hull et al., 2019) and following MCC950 treatment, a significant decrease in serum insulin levels were detected (-38%, $p<0.01$, Fig. 1j), but no changes were found in PLB_{WT} mice (+55%, $p>0.05$, Fig. 1j).

3.2 Circadian activity, habituation and motor function

Motor coordination and motor learning tests using a RotaRod task following MCC950 treatment in PLB_{WT} and $PLB2_{TAU}$ mice at 8-month of age revealed that only PLB_{WT} mice displayed motor learning across the eight trials, independently of treatment (+30%, $p<0.05$, $F(1, 18) = 8.089$, Fig. 2a&b). There was no significant improvement in motor learning in $PLB2_{TAU}$ mice in either treatment or vehicle group. As in a previous study (Hull et al., 2019), analysis of motor activity during the 3 hour habituation period to a novel environment, revealed a significant reduction in activity in vehicle treated $PLB2_{TAU}$ mice cf. controls (Fig. 2c). Data were fitted to an exponential decay function which indicated a significant decline in the plateau of $PLB2_{TAU}$ mice and in the rate at which motor activity declined (K) in $PLB2_{TAU}$ mice compared to vehicle treated WT controls was detected ($p<0.01$, $F(1, 318) = 7.95$, $p<0.0001$, $F(1, 318) = 18.20$, respectively). No differences were exhibited in PLB_{WT} mice following MCC950 treatment cf. vehicle treated controls (Fig. 2d). Following MCC950 treatment analysis of the motor activity plateau in $PLB2_{TAU}$ mice revealed a slight but significant increase cf vehicle ($p<0.05$, $F(1, 335) = 5.351$, Fig. 2e). The overall decline in motor activity in $PLB2_{TAU}$ mice was further confirmed based on the reduction in the mean hourly activity across 24 hours, however, no differences were detected in either genotype following MCC950 treatment relative to vehicle treated controls (Fig. 2f).

3.3 Tau and inflammatory markers in the brain

$PLB2_{TAU}$ mice express mutated human tau (hTauP301L + R406W) resulting in increased levels of phosphorylated tau at both CP-13 and PHF-1 epitopes at 6 months of age (Hull et al., 2019; Koss et al., 2016). We here first compared gene expression of mouse and human tau following MCC950 treatment using qPCR. Quantitative PCR analysis of mRNA isolated from brain tissue indicated that there were no changes in mouse tau expression following

treatment or indeed between genotypes at 8 months of age (Fig.3b). Analysis of human tau mRNA expression also confirmed stable tau expression following MCC950 treatment in $PLB2_{TAU}$ mice (Fig. 3c). Following this, we analysed protein levels of tau phosphorylation in brain tissue following MCC950 treatment in both PLB_{WT} and $PLB2_{TAU}$ mice at 8 months of age (Fig. 3d-f). Total tau levels quantified by the AT-5 antibody (3 bands) were unaltered in both genotypes following treatment (Fig.3d). Subsequently, we investigated phospho-tau levels in the soluble protein fraction. We confirmed increased levels of phospho-tau pathology at the PHF1 epitope (Ser396/ Ser404) in $PLB2_{TAU}$ mice compared to WT controls, both in vehicle and MCC950 treated mice (+100%, $p<0.0001$, $F(1, 40) = 24.85$, Fig.3e). There was a slight reduction in PHF1 levels in MCC950 treated $PLB2_{TAU}$ mice, but this did not reach significance ($p=0.1617$). Similar changes in tau phosphorylation were observed for the CP-13 epitope (Ser202), with increased levels of tau phosphorylation in vehicle treated $PLB2_{TAU}$ mice (+76%, $p<0.01$, $F(1, 38) = 2.248$, Fig. 3f), and again a minor, not significant reduction following treatment ($p=0.436$). However, it is noteworthy that the $PLB2_{TAU}$ treatment group no longer differed significantly from both WT controls and the WT MCC905 cohort ($p>0.05$), indicative of a normalisation and hence a beneficial effect of MCC905 on P-Tau levels in the transgenic mice.

3.4 Insulin signalling in the brain and peripheral tissue

Next, we investigated changes in insulin signalling in peripheral and brain tissue from PLB_{WT} and $PLB2_{TAU}$ mice following MCC950 treatment by probing for markers of the insulin signalling pathway (Fig. 4e and Suppl. Table 3). Protein analysis in skeletal muscle, a principal site of glucose uptake, showed similar changes in vehicle treated $PLB2_{TAU}$ mice as reported previously (Hull et al., 2019). A significant increase in phosphorylated IRβ

(Tyr1162/1163, relative to total expression) was detected in vehicle treated $PLB2_{TAU}$ mice cf. WT control (+38%, $p<0.01$, $F(1, 39) = 3.159$, Fig. 4b). Following MCC950 treatment, a decrease was observed (-21%, $p<0.05$, $F(1, 39) = 8.506$, Fig.4a). Total expression of the downstream marker IRS1 was significantly reduced in vehicle treated $PLB2_{TAU}$ mice at 8 months of age compared to vehicle treated PLB_{WT} controls (-46%, $p<0.01$, $F(1, 39) = 9.986$); MCC950 treatment let to a normalisation of IRS1 protein expression (+79%, $p<0.01$, $F(1, 39) = 7.774$). Furthermore, protein levels of phosphorylated JNK were elevated in vehicle treated $PLB2_{TAU}$ mice (+44%, $p<0.05$), but remained unchanged, following MCC950 in both PLB_{WT} and $PLB2_{TAU}$ (Fig.4b). Vehicle treated $PLB2_{TAU}$ mice had lower levels of phosphorylated AKT and phosphorylated ribosomal S6 compared to WT vehicle controls (-30%, $p=0.056$, -33%, $p=0.06$, respectively), indicative of muscle insulin resistance. Following MCC950 treatment, protein levels of phosphorylated ribosomal S6 were unchanged in PLB_{WT} mice. A significant decrease of phosphorylated AKT compared to vehicle treated controls was also detected (-38%, $p<0.05$). Protein levels of phosphorylated AKT and phosphorylated ribosomal S6 were significantly elevated in $PLB2_{TAU}$ mice, indicating normalisation after treatment (+48%, $p<0.05$, +83%, $p<0.05$, respectively, Fig.4b). No change occurred in overall total levels for IRβ, JNK, AKT and ribosomal S6 (Suppl. Fig. 2).

Analysis of insulin signalling in liver tissue following MCC950 treatment revealed no significant changes in expression of phosphorylated IRβ (Tyr 1163/1163) relative to total levels in both vehicle and MCC950 treatment groups (Fig.4c). IRS levels in PLB_{WT} mice were unaffected by treatment. However, there was a trend for increased levels in $PLB2_{TAU}$ mice following MCC950 treatment (+31%, $p=0.09$), suggesting some normalisation of insulin signalling. Protein levels of phosphorylated AKT and phosphorylated ribosomal S6 were reduced in vehicle treated $PLB2_{TAU}$ mice compared to WT controls (~25%, $p<0.05$), both

markers were not significantly affected by MCC950 as such but were however no longer significantly decreased c.f. controls. Phosphorylated JNK was elevated in vehicle treated $PLB2_{TAU}$ mice (+38%, p=0.0239) while there was a trend for diminished phosphorylated JNK in $PLB2_{TAU}$ mice only following MCC950 treatment (-37%, p=0.0617). No change in overall total levels for IRβ, JNK, AKT and ribosomal S6 (Suppl. Fig. 2) in both PLB_{WT} and $PLB2_{TAU}$ mice were detected.

Next, we examined insulin signalling in whole-brain tissue (Fig. 4d). Protein levels of phosphorylated IRβ (relative to total expression) were elevated in vehicle treated $PLB2_{TAU}$ mice compared to WT controls (+46%, p<0.01). Levels of phosphorylated IRβ were unaffected by treatment. Total IRS1 remained unaffected by MCC950 treatment in both genotypes but an overall genotype effect was seen in $PLB2_{TAU}$ mice (-~30%, p<0.01, F (1, 40) = 9.382). In contrast to peripheral tissues, phosphorylated AKT (+29%, p<0.01) and ribosomal S6 (+38%, p<0.01) were elevated in vehicle control $PLB2_{TAU}$ mice, and this was not affected by treatment in either PLB_{WT} and $PLB2_{TAU}$ mice. Analysis of phosphorylated JNK in brain tissue revealed a significant increase in vehicle treated $PLB2_{TAU}$ mice (+20%, p<0.05), but no effect of treatment was detected. Protein levels of total IRβ, JNK, AKT and ribosomal S6 (Suppl. Fig. 2) in PLB_{WT} mice remained unaffected by MCC950 (Fig 4d).

3.5 ER stress in liver and brain tissue

ER stress, reported to be a molecular link between obesity and the development of T2D, as well as being prominent in dementia (Ozcan, 2004), was next investigated (see also Suppl. Table 5). In liver, the mRNA expression of the ER chaperone, BiP, was significantly elevated in vehicle treated $PLB2_{TAU}$ mice compared to PLB_{WT} controls (+60%, p<0.0001, Fig. 5a), and significantly reduced by C950 treatment (-18%, p<0.05). There was no such change in PLB_{WT}

mice. No significant alterations were detected in gene expression of eIF2α or CHOP, but an overall genotype effect in expression of IRE1α was seen in $PLB2_{TAU}$ mice compared to WT controls (mRNA +54%, $p<0.01$, $F(1, 39) = 9.629$). The most robust difference detected in $PLB2_{TAU}$ mice vs. controls was a dramatic increase in ATF6 expression (+195%, $p<0.0001$). Here, MCC950 treatment trended towards a lowering of ATF6 levels in $PLB2_{TAU}$ mice, but not in PLB_{WT} controls (-23%, $p=0.08$). Changes in ER stress were further confirmed at protein level (Fig. 5d): A significant increase in BiP for vehicle control $PLB2_{TAU}$ mice compared to WT controls (+72%, $p<0.01$) was detected, and BiP levels were significantly lowered following MCC950 treatment (-18%, $p<0.05$). Phosphorylated eIF2α (+58%, $p<0.01$, $F(1, 39) = 8.485$) and phosphorylated IRE1α (+78%, $p<0.0001$, $F(1, 39) = 29.69$) showed an overall genotype effect in $PLB2_{TAU}$ mice but no effect of treatment in either genotype (Fig. 5.d).

Following this, we next determined alterations in ER stress markers at gene and protein level in brain tissue of PLB_{WT} and $PLB2_{TAU}$ mice (Fig.5b, e). In cortical tissue, and in contrast to liver tissue, a reduction in brain BiP expression (-45%, $p<0.01$, Fig. 5b) as well as eIF2α was detected in vehicle treated $PLB2_{TAU}$ mice c.f. controls (-27%, $p<0.05$). No changes were found in PLB_{WT} following treatment for eIF2α, but an overall treatment effect on mRNA expression of BiP was revealed, with an increased expression in both PLB_{WT} (+18%, $p<0.05$, $F(1, 39) = 4.640$) and $PLB2_{TAU}$ mice (+40%, $p<0.05$, $F(1, 39) = 4.640$). Analysis of mRNA expression in CHOP and ATF6 suggested no significant changes in either genotype following treatment, but an overall treatment effect of MCC950 on IRE1α expression, with an increase in both PLB_{WT} and $PLB2_{TAU}$ mice (+~20%, $p<0.05$, $F(1, 39) = 6.470$).

Western blot data confirmed changes in ER stress related markers (Fig. 5e), i.e. a reduction in BiP protein levels (-36%, $p<0.01$), phosphorylated eIF2α (-32%, $p<0.01$) and

phosphorylated IRE1α (-26%, p<0.05) in vehicle treated $PLB2_{TAU}$ mice compared to age-matched WT controls. Here, an overall treatment effect was again detected for both phosphorylated IRE1α and BiP with increased protein levels in PLB_{WT} and $PLB2_{TAU}$ mice compared to vehicle treated controls, yet no changes in phosphorylated eIF2α protein levels following treatment. It is of interest that MCC950 treatment had normalised levels of all ER stress markers to those of WT vehicle controls (P>0.05).

Overall, the tissue-specific ER phenotype of $PLB2_{TAU}$ mice, and the normalisation of particularly BiP by MCC950, independent of the directional shift in liver and brain in vehicle $PLB2_{TAU}$ mice cf. WT, is intriguing.

3.6 Inflammatory changes in the brain and peripheral tissue

We next determined inflammatory markers in liver tissue of PLB_{WT} and $PLB2_{TAU}$ mice following MCC950 treatment (Fig. 6, and Suppl.Table 4). The mRNA expression of NLRP3 was not affected *per se* by genotype or treatment (Fig. 6a), this was further confirmed at protein level (Fig.6d). A strong trend for increased expression of IL-18 was obtained in vehicle treated $PLB2_{TAU}$ mice compared to WT controls (+50%, p=0.06, Fig. 6a), but no treatment effect was detected in either group, though WT and transgenic IL-18 expression levels were identical post-treatment (p>0.05). An overall genotype effect of enhanced IL-1β expression was also detected in $PLB2_{TAU}$ mice (+17%, p<0.01, F (1, 39) = 7.736), but not affected by treatment in either genotype (Fig. 6a). TNFα, a priming signal for NLRP3, was strongly elevated in vehicle treated $PLB2_{TAU}$ mice compared to WT controls (+55%, p<0.01). Importantly, TNFα and NFκB mRNA expression displayed an overall treatment effect in both genotypes (TNFα : -20%, p<0.05, F (1, 39) = 5.773, NFκB: -31%, p<0.05, F (1, 39) = 5.130). At protein level, an overall treatment effect was also confirmed based on changes in pro-

caspase 1 (F (1,33) = 13.84, Fig 6d), alongside an overall genotype effect (F (1,33)= 4.859) in $PLB2_{TAU}$ mice. Though no gross difference in caspase-1 p10 was found in liver tissue of $PLB2_{TAU}$ mice vs WT, a genotype x treatment interaction ($p<0.05$, F (1,29) = 5.546)) was seen for pro-IL1β, due to higher basal levels in transgenic mice, reduced in $PLB2_{TAU}$ mice but not WT controls post-treatment. Together, our data suggest heightened liver inflammation in $PLB2_{TAU}$ mice, which was partially normalised by MCC950 treatment.

In the brain, a basal increase in inflammatory status of $PLB2_{TAU}$ mice was indicated by differences in gene expression (Fig. 6b), i.e. elevations in NLRP3 (+30%, $p<0.05$, F (1, 39) = 5.422), TNFα (+29%, $p<0.05$, F (1, 39) = 5.953, Fig. 6b), and NFκB (+36%, $p<0.05$, F (1, 39) = 7.103) expression in cortical tissue of $PLB2_{TAU}$ mice relative to WT controls. Though no gross effect of MCC950 was observed and mRNA expression of Interleukin 1β (IL-1β) remained unaffected, treatment effects were indicated by IL-18 expression, significantly elevated in vehicle treated $PLB2_{TAU}$ mice compared to WT controls (+36%, $p<0.05$), and trending to be reduced by MCC950 (-19%, $p=0.07$). Normalisation of IL-18 and NFκB expression post treatment was further confirmed as levels were equal to WT controls ($p>0.05$).

At protein level, no difference in NLRP3 was found for brain tissue of $PLB2_{TAU}$ mice vs WT controls, and no effect of MCC950 treatment (Fig. 6e). Unfortunately, WB detection of caspase and IL-1 protein levels was not reliably possible in brain tissue homogenates (data not shown), likely due to tissue-and cell-type specific expression. As NLRP3 activation in the brain may be specific to microglia activation (Deora et al., 2020), we thus analysed levels of activated microglia (IBA1). An overall significant reduction of IBA1 was identified in $PLB2_{TAU}$ mice compared to PLB_{WT} (-30%, $p<0.05$, F (1, 26) = 4.743). Though there was no gross effect of treatment in either genotype, we obtained a genotype x treatment interaction ($p=0.0255$,

F (1,29) = 5.546) and Iba-1 levels normalised to WT levels ($p>0.05$). Conversely, higher GFAP levels indicated astrogliosis in $PLB2_{TAU}$ mice cf WT controls (+100%, $p<0.0001$, F (1, 26) = 36.61), here, no effect of treatment was apparent in either genotype (Fig. 6e).

4. Discussion

In the present study, we investigated the effects of MCC950, a novel small-molecule NLRP3 inhibitor, in hTAU expressing $PLB2_{TAU}$ mice at 8 months of age, alongside age-matched PLB_{WT} controls. MCC950 has recently been investigated as a potential therapeutic agent to reverse AD and T2D-related pathologies. Due to the novelty of this treatment, the efficacy in FTD models remained unknown, though a recent report strongly implicated the NLRP3 inflammasome in tau pathology (Ising et al., 2019). Here, we report that MCC950 treatment improved insulin sensitivity and reduced circulating plasma insulin levels in $PLB2_{TAU}$ mice. MCC950 also resulted in changes in central and peripheral insulin signalling, inflammatory markers and ER stress signalling, both peripherally and centrally while CNS phospho-Tau levels were partially normalised.

It is important to note that MCC950 treatment did not inhibit the heightened levels of NLRP3 in brain or liver tissue of $PLB2_{TAU}$ mice, which is in accordance with previous reports (Kammoun et al., 2018). We suggested that although protein and mRNA expression of the receptor itself were unaltered in $PLB2_{TAU}$ mice, downstream pathways directly associated with the inflammasome were affected. As a NLRP3 inhibitor, total protein levels

of NLRP3 does not need to change due to MCC950 inhibition, instead, effects on downstream pathways are likely to be affected. Accordingly, in the brain both IL-1β and IL-18, which are regulated by the NLRP3 inflammasome (Felderhoff-Mueser et al., 2005; Freeman and Ting, 2016) were reduced with treatment.

As previously reported (Hull et al., 2019), $PLB2_{TAU}$ mice exhibit impaired glucose handling, increased hepatic gluconeogenesis and insulin resistance assumed as a result of neuronal expression of human mutated tau, disturbing insulin signalling and protein handling. MCC950 treatment did not affect body weight or body composition, and no gross changes were observed in behaviour, systemic glucose homeostasis or hepatic gluconeogenesis in $PLB2_{TAU}$ mice or PLB_{WT} controls, which is consistent with the results from a previous study (Kammoun et al., 2018). However, treatment significantly improved insulin sensitivity and decreased serum insulin levels in $PLB2_{TAU}$ mice. This is in line with previous reports that MCC950 enhanced insulin sensitivity in db/db mice (Zhai et al., 2018). Zhai and colleagues hypothesised these effects may be linked to the inhibition of nuclear factor kappa-light-chain-enhancer of activated B cells (NF-κB) signalling. Insulin resistance is increasingly associated with systemic chronic inflammation induced by various pro-inflammatory cytokines including, but not limited to, interleukin (IL) – 18, IL-1β, tumour necrosis factor-α (TNF-α) and NFκB (Dandona et al., 2004, 1998; Mantzoros et al., 1997; Ofei et al., 1996). These inflammatory cytokines are released following the activation of the inflammasome, which recruits and activates cytokine signalling proteins, to ultimately inhibit insulin receptor signalling by serine phosphorylation of IRS1/2 diminishing downstream insulin signalling (Akash et al., 2013; Donath and Shoelson, 2011; Fève and Bastard, 2012; Kahn et al., 2006; Shoelson et al., 2006). In agreement with our observations, previous data have shown that inhibition of NFκB can improve insulin resistance in mouse

models of diabetes (Arkan et al., 2005; Baker et al., 2011; Yekollu et al., 2011; Zhang et al., 2010), further confirming the role of NLRP3 inflammasome in metabolic regulation.

Despite mounting evidence suggesting a relationship between neurodegenerative diseases and neuroinflammation, there is a scarcity of studies assessing inflammasome interventions in tauopathy mouse models of dementia. Modulating inflammation offers the possibility to investigate inflammatory components and evaluate how inflammatory mediators contribute to tau pathology. Recently, Ising and colleagues reported that inhibition of NLRP3 inflammasome through crossing of the established Tau22 mice with mice deficient in caspase 1 (Ising et al., 2019) resulted in a reduction of hippocampal tau phosphorylation, which was suggested to be a result of a reduction in key tau kinases and phosphatases such as protein phosphatase 2 (PP2A) (Ising et al., 2019). In contrast, our data showed that MCC950 was unable to alter tau gene expression and only partially normalised tau phosphorylation in brain tissue of $PLB2_{TAU}$ mice. With regards to pathological tau, particularly the PHF1 epitope showed a positive normalisation, which may suggest that either a longer treatment or higher concentration may be required to bring about more significant changes in tau pathology in $PLB2_{TAU}$ mice. Though the inhibition of the NLRP3 inflammasome was not sufficient to fully correct changes in tau pathology (and other factors that may be driving the progression of the disease in this mouse model of FTD), our data are indicative of a positive overall impact on FTD pathology.

Moreover, we detected alterations in insulin signalling in both peripheral and brain tissue in $PLB2_{TAU}$ mice following MCC950 treatment. In skeletal muscle (primary site of insulin resistance), $PLB2_{TAU}$ mice displayed elevated levels of IRS1, AKT and ribosomal S6 following MCC950 treatment, signifying decreased insulin resistance and increased insulin sensitivity in skeletal muscle. This finding is consistent with other studies suggesting

improved insulin sensitivity in skeletal muscle following an anti-inflammatory treatment in a model of T2D (Dagdeviren et al., 2016; Hong et al., 2009). Hong et al. revealed that IL-10 (anti-inflammatory cytokine) treatment protects against diet-induced insulin resistance in C57BL/6 mice. We therefore suggest that MCC950 can inhibit inflammation thus improving metabolic status and insulin sensitivity in skeletal muscle. The inhibition of TNFα could potentially restore impaired insulin signalling in the $PLB2_{TAU}$ mice by alleviating the inhibitory effects of JNK on IRS1 (de Alvaro et al., 2004; Gao et al., 2002; Yuan et al., 2001). This same inhibitory effect on JNK was also detected in liver and brain tissue of $PLB2_{TAU}$ mice. However, no overall gross improvement in blood glucose levels were found. In neurodegenerative diseases such as FTD, ER stress can cause inflammatory reactions via activation of NFκB (Kaneko et al., 2003). Yet, there remains a gap in our knowledge regarding the cell-specific mechanisms by which ER stress mediates inflammation. Hu et al. found a link between ER stress and TNFα through NF-κB signalling. They revealed that inhibiting NFκB and TNFα signalling resulted in a reduction in ER stress-induced apoptosis (Hu et al., 2006).

As previously reported (Hull et al., 2019), $PLB2_{TAU}$ mice present with a downregulation of ER stress-related markers in brain tissue compared to WT controls. Following MCC950 treatment, our data indicated a subtle upregulation of ER stress markers, BiP and IRE1α in brain tissue of $PLB2_{TAU}$ mice, suggesting that alleviating inflammation response could potentially repair the protective ER function. The changes in ER stress signalling in the brain do not necessarily follow the changes in peripheral tissue, and a number of tissue-specific ER stress pathways were clearly identified here (e.g. enhanced ATF6 expression in liver, reduced BiP, eIF2α and IRE-1α in brain). Elevated ER stress in peripheral tissues is increasingly acknowledged as an important mechanism in the

development of T2D, and plays a key role in insulin resistance (Ozcan, 2004). While alterations of specific ER related markers such as BiP and eIF2α were for example reported in a diabetic mouse model following the inhibition of the NLRP3 inflammasome (Lerner et al., 2012), such pathways were not explored in the Tau22 model (Ising et al., 2019). Our data would suggest that inflammasome and ER-targeting treatments may have to be tailored towards tissue-specific pathways to achieve greater efficacy.

In summary, our data provided valuable insights into the role of NLRP3 and the efficacy of MCC950 in the treatment of FTD and T2D-related pathologies. Even though MCC950 did not normalise all aspects of the diabetic phenotype of $PLB2_{TAU}$ mice, we demonstrated a number of beneficial effects such as increased insulin sensitivity, reversal of skeletal muscle insulin resistance, reduction in various inflammatory markers, partial normalisation of phospho-tau levels and ER stress markers of $PLB2_{TAU}$ mice.

Acknowledgments

This study was supported by ARUK project grant PG2017B-11 and ARUK summer scholarship funding from the Scottish ARUK network. The authors would like to thank Prof. Gernot Riedel for his support of the *in vivo* experimentation.

Conflict of Interest

The authors have no conflict of interest to report.

Figure and Table Legends

Figure 1: Metabolic phenotypes of PLB_{WT} and $PLB2_{TAU}$ mice following MCC950 treatment. A two-way ANOVA was performed for quantification of (A) Body weights over the 12-week treatment period and (B) change in body weight (in %). (C) Fat and lean body composition determined via EchoMRI. (D-E) Glucose tolerance tests (GTT) and quantification of area under the curve (AUC) for total glycaemic excursions. (F-G) Insulin tolerance tests (ITTs) and quantification of AUC. (H-I) Pyruvate tolerance tests (PTTs) and quantification of AUC. (J) Quantification of insulin levels in serum. PLB_{WT} (vehicle) n=5, PLB_{WT} (MCC950) n=5, $PLB2_{TAU}$ (vehicle) n=5 and $PLB2_{TAU}$ (MCC950) n=5. Data are shown as scatter as well as means +/- SEM, significances are given as ****p<0.0001, ***p<0.001, **p<0.01 &*p<0.05. $: treatment effect in both PLB_{WT} and $PLB2_{TAU}$ mice . N.S. = not significant.

Figure 2: Behavioural phenotype of PLB_{WT} and $PLB2_{TAU}$ mice during PhenoTyper home cage activity analysis and RotaRod task following MCC950 treatment. Two-way ANOVA was performed for quantification of (A) Latency to fall from RotaRod and (B) Motor learning (trial 1 vs trial 8) during RotaRod task. (C-E) Nonlinear regression analysis (one-phase decay) of activity (distanced moved, cm / 10 mins) during the 3h habituation period in the PhenoTyper home cage. Results for the goodness of the fit as well as statistical comparison between groups for: initial novelty-induced exploration at time 0 (Y0), exploration during plateau phase (stable y-axis level) as well as the rate constant of decline (K, inverse of time constant tau) as a proxy for the speed of habituation are indicated within the graphs. (F) Average hourly activity over 24 hours. PLB_{WT} (vehicle) n=13, PLB_{WT} (MCC950) n=10, $PLB2_{TAU}$ (vehicle) n=11 and $PLB2_{TAU}$ (MCC950) n=11. Individual data points and means (+/- SEM) are

illustrated, significances are indicated as ***p<0.001, **p<0.01, *p<0.05. N.S. = not significant.

Figure 3: Expression of phosphorylated tau in PLB_{WT} and $PLB2_{TAU}$ mice following MCC950 or vehicle treatment. (A) Representative Western blots of phosphorylated tau in both PLB_{WT} and $PLB2_{TAU}$ male mice. (B) Quantification of mouse Tau expression via qPCR and (C, two-way ANOVA) and human Tau (student's t-tests since no hTau was detected in WT samples) expression in transgenic mice. (D) Quantification of total tau (AT5) protein levels. A two-way ANOVA was performed for quantification of (E) individual bands and total expression for PHF1 positive tau species (relative to total Tau) and (F) individual bands and total phospho-tau (CP13) levels relative to total Tau. PLB_{WT} (vehicle) n=13, PLB_{WT} (MCC950) n=10, $PLB2_{TAU}$ (vehicle) n=11 and $PLB2_{TAU}$ (MCC950) n=11. Data are shown as scatter (individual data points) as well as means +/- SEM, significances are indicated as ***p<0.001, **p<0.01 &*p<0.05. N.S. = not significant.

Figure 4: Insulin signalling in the brain and peripheral tissues in PLB_{WT} and $PLB2_{TAU}$ mice following MCC950 or vehicle treatment. (A) Representative Western blots for insulin signalling markers in the muscle, liver and brain. Significances (two-way ANOVA) are given for (B) muscle, (C) liver and (D) brain. (E) Simplified schematic illustrating insulin signalling cascade investigated. All phospho markers are expressed relative to total expression. PLB_{WT} (vehicle) n=13, PLB_{WT} (MCC950) n=10, $PLB2_{TAU}$ (vehicle) n=11 and $PLB2_{TAU}$ (MCC950) n=11. Individual data points are shown as well as means +/- SEM, significances are given as : # overall genotype effect, ***p<0.001, **p<0.01, *p<0.05. N.S. = not significant.

Figure 5: ER stress gene expression and protein levels in liver and brain tissue of PLB_{WT} and $PLB2_{TAU}$ mice following MCC950 or vehicle treatment. Gene expression of ER stress related markers in (A) liver and (B) brain tissue. (C) Western blot examples of phosphorylated IRE1α, BiP, and phosphorylated eIF2α in liver and brain tissue. Two-way ANOVAs were performed for quantification of ER stress markers in (D) liver and (E) brain tissue. (F) Simplified ER stress signalling cascade, illustrating pathways probed here. All phospho markers are expressed relative to total expression. PLB_{WT} (vehicle) n=13, PLB_{WT} (MCC950) n=10, $PLB2_{TAU}$ (vehicle) n=11 and $PLB2_{TAU}$ (MCC950) n=11. # genotype effect, $ treatment effect, ****p<0.0001, **p<0.01, *p<0.05.

Figure 6: Inflammatory gene expression and protein levels in liver and brain tissue of PLB_{WT} and $PLB2_{TAU}$ mice following MCC950 or vehicle treatment. Gene expression in inflammatory related markers in (A) liver and (B) brain. (C) Western blots of inflammatory markers in both liver and brain tissue. (D&E) Two-way ANOVA was performed for quantification of ER stress markers in liver and brain tissue. PLB_{WT} (vehicle) n=13, PLB_{WT} (MCC950) n=10, $PLB2_{TAU}$ (vehicle) n=11 and $PLB2_{TAU}$ (MCC950) n=11. # genotype effect, $ treatment effect, **p<0.01, *p<0.05.

Supplementary Table 1 Antibodies used for protein expression quantification, "p-"= phospho-specific

Supplementary Table 2 List of primers used for qPCR analysis.

Supplementary Table 3 Insulin signalling results summary table.

Supplementary Table 4 Inflammation results summary table.

Supplementary Table 5 ER stress results summary table.

Supplementary Figure 1 Schematic of study timeline for MCC950 and vehicle treatment in $PLB2_{TAU}$ and PLB_{WT} controls.

Supplementary Figure 2 Total protein levels in the brain vs periphery in PLB_{WT} and $PLB2_{TAU}$ mice following vehicle and MCC950 treatment. (A) Representative Western blots for insulin signalling and ER stress markers. Two-way ANOVAs were performed for quantification of total ER stress markers in the (B) liver and (C) brain. Quantification of insulin signalling markers in the (D) muscle (E) liver and (F) brain. PLB_{WT} (vehicle) n=13, PLB_{WT} (MCC950) n=10, $PLB2_{TAU}$ (vehicle) n=11 and $PLB2_{TAU}$ (MCC950) n=11. N.S. = not significant.

Supplementary Figure 3 Coomassie loading controls for all blots.

1.6 References

Akash, M.S.H., Rehman, K., Chen, S., 2013. Role of inflammatory mechanisms in pathogenesis of type 2 diabetes mellitus. J. Cell. Biochem. https://doi.org/10.1002/jcb.24402

Arkan, M.C., Hevener, A.L., Greten, F.R., Maeda, S., Li, Z.-W., Long, J.M., Wynshaw-Boris, A., Poli, G., Olefsky, J., Karin, M., 2005. IKK-β links inflammation to obesity-induced insulin resistance. Nat. Med. 11, 191–198. https://doi.org/10.1038/nm1185

Baker, R.G., Hayden, M.S., Ghosh, S., 2011. NF-kB, Inflammation, and Metabolic Disease. Cell Metab. 13, 11–22. https://doi.org/10.1016/j.cmet.2010.12.008.NF-

Bello-Chavolla, O.Y., Antonio-Villa, N.E., Vargas-Vázquez, A., Ávila-Funes, J.A., Aguilar-Salinas, C.A., 2019. Pathophysiological Mechanisms Linking Type 2 Diabetes and Dementia: Review of Evidence from Clinical, Translational and Epidemiological Research. Curr. Diabetes Rev. 15, 456–470. https://doi.org/10.2174/1573399815666190129155654

Broz, P., Dixit, V.M., 2016. Inflammasomes: Mechanism of assembly, regulation and signalling. Nat. Rev. Immunol. https://doi.org/10.1038/nri.2016.58

Coll, R.C., Hill, J.R., Day, C.J., Zamoshnikova, A., Boucher, D., Massey, N.L., Chitty, J.L., Fraser, J.A., Jennings, M.P., Robertson, A.A.B., Schroder, K., 2019. MCC950 directly targets the NLRP3 ATP-hydrolysis motif for inflammasome inhibition. Nat. Chem. Biol. 15, 556–559. https://doi.org/10.1038/s41589-019-0277-7

Coll, R.C., Robertson, A.A.B., Chae, J.J., Higgins, S.C., Muñoz-Planillo, R., Inserra, M.C., Vetter, I., Dungan, L.S., Monks, B.G., Stutz, A., Croker, D.E., Butler, M.S., Haneklaus, M., Sutton, C.E., Núñez, G., Latz, E., Kastner, D.L., Mills, K.H.G., Masters, S.L., Schroder, K., Cooper, M.A., O'neill, L.A.J., 2015. A small molecule inhibitior of the NLRP3 inflammasome is a potential therapeutic for inflammatory diseases HHS Public Access. Nat Med 21, 248–255. https://doi.org/10.1038/nm.3806

Dagdeviren, S., Jung, D.Y., Lee, E., Friedline, R.H., Noh, H.L., Kim, J.H., Patel, P.R., Tsitsilianos, N., Tsitsilianos, A. V., Tran, D.A., Tsougranis, G.H., Kearns, C.C., Uong, C.P., Kwon, J.Y., Muller, W., Lee, K.W., Kim, J.K., 2016. Altered Interleukin-10 Signaling in Skeletal

Muscle Regulates Obesity-Mediated Inflammation and Insulin Resistance. Mol. Cell. Biol. 36, 2956–2966. https://doi.org/10.1128/MCB.00181-16

Dandona, P., Aljada, A., Bandyopadhyay, A., 2004. Inflammation: The link between insulin resistance, obesity and diabetes. Trends Immunol. https://doi.org/10.1016/j.it.2003.10.013

Dandona, P., Weinstock, R., Thusu, K., Abdel-Rahman, E., Aljada, A., Wadden, T., 1998. Tumor necrosis factor-alpha in sera of obese patients: Fall with weight loss. J. Clin. Endocrinol. Metab. 83, 2907–2910. https://doi.org/10.1210/jc.83.8.2907

Daniels, M.J.D., Rivers-Auty, J., Schilling, T., Spencer, N.G., Watremez, W., Fasolino, V., Booth, S.J., White, C.S., Baldwin, A.G., Freeman, S., Wong, R., Latta, C., Yu, S., Jackson, J., Fischer, N., Koziel, V., Pillot, T., Bagnall, J., Allan, S.M., Paszek, P., Galea, J., Harte, M.K., Eder, C., Lawrence, C.B., Brough, D., 2016. Fenamate NSAIDs inhibit the NLRP3 inflammasome and protect against Alzheimer's disease in rodent models. Nat. Commun. 7, 12504. https://doi.org/10.1038/ncomms12504

de Alvaro, C., Teruel, T., Hernandez, R., Lorenzo, M., 2004. Tumor Necrosis Factor α Produces Insulin Resistance in Skeletal Muscle by Activation of Inhibitor κB Kinase in a p38 MAPK-dependent Manner. J. Biol. Chem. 279, 17070–17078. https://doi.org/10.1074/jbc.M312021200

Dempsey, C., Rubio Araiz, A., Bryson, K.J., Finucane, O., Larkin, C., Mills, E.L., Robertson, A.A.B., Cooper, M.A., O'Neill, L.A.J., Lynch, M.A., 2017. Inhibiting the NLRP3 inflammasome with MCC950 promotes non-phlogistic clearance of amyloid-β and cognitive function in APP/PS1 mice. Brain. Behav. Immun. 61, 306–316. https://doi.org/10.1016/j.bbi.2016.12.014

Deora, V., Lee, J.D., Albornoz, E.A., McAlary, L., Jagaraj, C.J., Robertson, A.A.B., Atkin, J.D., Cooper, M.A., Schroder, K., Yerbury, J.J., Gordon, R., Woodruff, T.M., 2020. The microglial NLRP3 inflammasome is activated by amyotrophic lateral sclerosis proteins. Glia 68, 407–421. https://doi.org/10.1002/glia.23728

Donath, M.Y., Shoelson, S.E., 2011. Type 2 diabetes as an inflammatory disease. Nat. Rev. Immunol. 11, 98–107. https://doi.org/10.1038/nri2925

Fan, Y., Du, L., Fu, Q., Zhou, Z., Zhang, J., Li, G., Wu, J., 2018. Inhibiting the NLRP3 Inflammasome With MCC950 Ameliorates Isoflurane-Induced Pyroptosis and Cognitive Impairment in Aged Mice. Front. Cell. Neurosci. 12, 426. https://doi.org/10.3389/fncel.2018.00426

Fekete, C., Vastagh, C., Dénes, Á., Hrabovszky, E., Nyiri, G., Kalló, I., Liposits, Z., Sárvári, M., 2019. Chronic Amyloid β Oligomer Infusion Evokes Sustained Inflammation and Microglial Changes in the Rat Hippocampus via NLRP3. Neuroscience 405, 35–46. https://doi.org/10.1016/j.neuroscience.2018.02.046

Felderhoff-Mueser, U., Schmidt, O.I., Oberholzer, A., Bührer, C., Stahel, P.F., 2005. IL-18: A key player in neuroinflammation and neurodegeneration? Trends Neurosci. https://doi.org/10.1016/j.tins.2005.06.008

Fève, B., Bastard, J.-P., 2012. The role of interleukins in insulin resistance and type 2 diabetes mellitus. Nat. Rev. Endocrinol. 8, 92–103. https://doi.org/10.1038/nrendo.2011.138

Freeman, L.C., Ting, J.P.Y., 2016. The pathogenic role of the inflammasome in neurodegenerative diseases. J. Neurochem. 136, 29–38. https://doi.org/10.1111/jnc.13217

Gao, Z., Hwang, D., Bataille, F., Lefevre, M., York, D., Quon, M.J., Ye, J., 2002. Serine phosphorylation of insulin receptor substrate 1 by inhibitor kappa B kinase complex. J. Biol. Chem. 277, 48115–48121. https://doi.org/10.1074/jbc.M209459200

Halle, A., Hornung, V., Petzold, G.C., Stewart, C.R., Monks, B.G., Reinheckel, T., Fitzgerald, K.A., Latz, E., Moore, K.J., Golenbock, D.T., 2008. The NALP3 inflammasome is involved in the innate immune response to amyloid-β. Nat. Immunol. 9, 857–865. https://doi.org/10.1038/ni.1636

Heneka, M.T., Kummer, M.P., Stutz, A., Delekate, A., Schwartz, S., Vieira-saecker, A., Griep, A., Axt, D., Remus, A., Tzeng, T., Gelpi, E., Halle, A., Korte, M., Latz, E., Golenbock, D.T., 2013. contributes to pathology in APP / PS1 mice. Nature 493, 674–678. https://doi.org/10.1038/nature11729

Hong, E.G., Hwi, J.K., Cho, Y.R., Kim, H.J., Ma, Z., Yu, T.Y., Friedline, R.H., Kurt-Jones, E.,

Finberg, R., Fischer, M.A., Granger, E.L., Norbury, C.C., Hauschka, S.D., Philbrick, W.M., Lee, C.G., Elias, J.A., Kim, J.K., 2009. Interleukin-10 prevents diet-induced insulin resistance by attenuating macrophage and cytokine response in skeletal muscle. Diabetes 58, 2525–2535. https://doi.org/10.2337/db08-1261

Hu, P., Han, Z., Couvillon, A.D., Kaufman, R.J., Exton, J.H., 2006. Autocrine tumor necrosis factor alpha links endoplasmic reticulum stress to the membrane death receptor pathway through IRE1alpha-mediated NF-kappaB activation and down-regulation of TRAF2 expression. Mol. Cell. Biol. 26, 3071–84. https://doi.org/10.1128/MCB.26.8.3071-3084.2006

Hull, C., Dekeryte, R., Koss, D.J., Crouch, B., Buchanan, H., Delibegovic, M., Platt, B., 2019. Knock-in of Mutated hTAU Causes Insulin Resistance, Inflammation and Proteostasis Disturbance in a Mouse Model of Frontotemporal Dementia. Mol. Neurobiol. 1–12. https://doi.org/10.1007/s12035-019-01722-6

Ising, C., Venegas, C., Zhang, S., Scheiblich, H., Schmidt, S. V, Vieira-Saecker, A., Schwartz, S., Albasset, S., McManus, R.M., Tejera, D., Griep, A., Santarelli, F., Brosseron, F., Opitz, S., Stunden, J., Merten, M., Kayed, R., Golenbock, D.T., Blum, D., Latz, E., Buée, L., Heneka, M.T., 2019. NLRP3 inflammasome activation drives tau pathology. Nature 575, 669–673. https://doi.org/10.1038/s41586-019-1769-z

Jiang, D., Chen, S., Sun, R., Zhang, X., Wang, D., 2018. The NLRP3 inflammasome: Role in metabolic disorders and regulation by metabolic pathways. Cancer Lett. https://doi.org/10.1016/j.canlet.2018.01.034

Kahn, S.E., Hull, R.L., Utzschneider, K.M., 2006. Mechanisms linking obesity to insulin resistance and type 2 diabetes. Nature 444, 840–846. https://doi.org/10.1038/nature05482

Kammoun, H.L., Allen, T.L., Henstridge, D.C., Barre, S., Coll, R.C., Lancaster, G.I., Cron, L., Reibe, S., Chan, J.Y., Bensellam, M., Laybutt, D.R., Butler, M.S., Robertson, A.A.B., O'Neill, L.A., Cooper, M.A., Febbraio, M.A., 2018. Evidence against a role for NLRP3-driven islet inflammation in db/db mice. Mol. Metab. 10, 66–73. https://doi.org/10.1016/j.molmet.2018.02.001

Kaneko, M., Niinuma, Y., Nomura, Y., 2003. Activation signal of nuclear factor-kappa B in response to endoplasmic reticulum stress is transduced via IRE1 and tumor necrosis factor receptor-associated factor 2. Biol. Pharm. Bull. 26, 931–5. https://doi.org/10.1248/bpb.26.931

Koss, D.J., Robinson, L., Drever, B.D., Plucińska, K., Stoppelkamp, S., Veselcic, P., Riedel, G., Platt, B., 2016. Mutant Tau knock-in mice display frontotemporal dementia relevant behaviour and histopathology. Neurobiol. Dis. 91, 105–123. https://doi.org/10.1016/j.nbd.2016.03.002

Latz, E., Xiao, T.S., Stutz, A., 2013. Activation and regulation of the inflammasomes. Nat. Rev. Immunol. 13, 397–411. https://doi.org/10.1038/nri3452

Lauretti, E., Li, J.G., Di Meco, A., Praticò, D., 2017. Glucose deficit triggers tau pathology and synaptic dysfunction in a tauopathy mouse model. Transl. Psychiatry 7, 1–9. https://doi.org/10.1038/tp.2016.296

Lee, H.M., Kim, J.J., Kim, H.J., Shong, M., Ku, B.J., Jo, E.K., 2013. Upregulated NLRP3 inflammasome activation in patients with type 2 diabetes. Diabetes 62, 194–204. https://doi.org/10.2337/db12-0420

Lerner, A.G., Upton, J.P., Praveen, P.V.K., Ghosh, R., Nakagawa, Y., Igbaria, A., Shen, S., Nguyen, V., Backes, B.J., Heiman, M., Heintz, N., Greengard, P., Hui, S., Tang, Q., Trusina, A., Oakes, S.A., Papa, F.R., 2012. IRE1α induces thioredoxin-interacting protein to activate the NLRP3 inflammasome and promote programmed cell death under irremediable ER stress. Cell Metab. 16, 250–264. https://doi.org/10.1016/j.cmet.2012.07.007

Liou CJ, Tong M, Vonsattel JP, de la Monte SM., 2019 Altered brain expression of insulin and insulin-like growth factors in frontotemporal lobar degeneration: Another degenerative disease linked to dysregulation of insulin metabolic pathways. *ASN Neuro*. 11:1759091419839515. doi:10.1177/1759091419839515

Mantzoros, C.S., Moschos, S., Avramopoulos, I., Kaklamani, V., Liolios, A., Doulgerakis, D.E., Griveas, I., Katsilambros, N., Flier, J.S., 1997. Leptin Concentrations in Relation to Body Mass Index and the Tumor Necrosis Factor-α System in Humans [1]. J. Clin. Endocrinol.

Metab. 82, 3408–3413. https://doi.org/10.1210/jcem.82.10.4323

Marciniak, E., Leboucher, A., Caron, E., Ahmed, T., Tailleux, A., Dumont, J., Issad, T., Gerhardt, E., Pagesy, P., Vileno, M., Bournonville, C., Hamdane, M., Bantubungi, K., Lancel, S., Demeyer, D., Eddarkaoui, S., Vallez, E., Vieau, D., Humez, S., Faivre, E., Grenier-Boley, B., Outeiro, T.F., Staels, B., Amouyel, P., Balschun, D., Buee, L., Blum, D., 2017. Tau deletion promotes brain insulin resistance. J. Exp. Med. 214, 2257–2269. https://doi.org/10.1084/jem.20161731

Mushtaq, G., Khan, J.A., Kumosani, T.A., Kamal, M.A., 2015. Alzheimer's disease and type 2 diabetes via chronic inflammatory mechanisms. Saudi J. Biol. Sci. 22, 4–13. https://doi.org/10.1016/j.sjbs.2014.05.003

Ofei, F., Hurel, S., Newkirk, J., Sopwith, M., Taylor, R., 1996. Effects of an engineered human anti-TNF-α antibody (CDP571) on insulin sensitivity and glycemic control in patients with NIDDM. Diabetes 45, 881–885. https://doi.org/10.2337/diab.45.7.881

Ozcan, U., 2004. Endoplasmic Reticulum Stress Links Obesity, Insulin Action, and Type 2 Diabetes. Science (80-.). 306, 457–461. https://doi.org/10.1126/science.1103160

Plucinska, K., Crouch, B., Koss, D., Robinson, L., Siebrecht, M., Riedel, G., Platt, B., 2014. Knock-In of Human BACE1 Cleaves Murine APP and Reiterates Alzheimer-like Phenotypes. J. Neurosci. 34, 10710–10728. https://doi.org/10.1523/JNEUROSCI.0433-14.2014

Primiano MJ, Lefker BA, Bowman MR, Bree AG, Hubeau C, Bonin PD, Mangan M, Dower K, Monks BG, Cushing L, Wang S, Guzova J, Jiao A, Lin L-L, Latz E, Hepworth D, Hall JP, 2016. Efficacy and Pharmacology of the NLRP3 Inflammasome Inhibitor CP-456,773 (CRID3) in Murine Models of Dermal and Pulmonary Inflammation. J. Immunol. 197, 2421–2433.

Qi, Y., Klyubin, I., Cuello, A.C., Rowan, M.J., 2018. NLRP3-dependent synaptic plasticity deficit in an Alzheimer's disease amyloidosis model in vivo. Neurobiol. Dis. 114, 24–30. https://doi.org/10.1016/j.nbd.2018.02.016

Rheinheimer, J., de Souza, B.M., Cardoso, N.S., Bauer, A.C., Crispim, D., 2017. Current role of the NLRP3 inflammasome on obesity and insulin resistance: A systematic review.

Metabolism 74, 1–9. https://doi.org/10.1016/j.metabol.2017.06.002

Robinson, L., Plano, A., Cobb, S., Riedel, G., 2013. Long-term home cage activity scans reveal lowered exploratory behaviour in symptomatic female Rett mice. Behav. Brain Res. 250, 148–156. https://doi.org/10.1016/j.bbr.2013.04.041

Shoelson, S.E., Lee, J., Goldfine, A.B., 2006. Inflammation and insulin resistance. J. Clin. Invest. 116, 1793–801. https://doi.org/10.1172/JCI29069

Španić, E., Langer Horvat, L., Hof, P.R., Šimić, G., 2019. Role of Microglial Cells in Alzheimer's Disease Tau Propagation. Front. Aging Neurosci. 11, 271. https://doi.org/10.3389/fnagi.2019.00271

Stancu, I.-C., Cremers, N., Vanrusselt, H., Couturier, J., Vanoosthuyse, A., Kessels, S., Lodder, C., Brône, B., Huaux, F., Octave, J.-N., Terwel, D., Dewachter, I., 2019. Aggregated Tau activates NLRP3–ASC inflammasome exacerbating exogenously seeded and non-exogenously seeded Tau pathology in vivo. Acta Neuropathol. 137, 599–617. https://doi.org/10.1007/s00401-018-01957-y

Stienstra, R., van Diepen, J.A., Tack, C.J., Zaki, M.H., van de Veerdonk, F.L., Perera, D., Neale, G.A., Hooiveld, G.J., Hijmans, A., Vroegrijk, I., van den Berg, S., Romijn, J., Rensen, P.C.N., Joosten, L.A.B., Netea, M.G., Kanneganti, T.-D., 2011. Inflammasome is a central player in the induction of obesity and insulin resistance. Proc. Natl. Acad. Sci. 108, 15324–15329. https://doi.org/10.1073/pnas.1100255108

Strachan, M.W.J., Reynolds, R.M., Frier, B.M., Mitchell, R.J., Price, J.F., 2008. The relationship between type 2 diabetes and dementia. Br. Med. Bull. 88, 131–146. https://doi.org/10.1093/bmb/ldn042

Tan, M.-S., Yu, J.-T., Jiang, T., Zhu, X.-C., Tan, L., 2013. The NLRP3 Inflammasome in Alzheimer's Disease. Mol. Neurobiol. 48, 875–882. https://doi.org/10.1007/s12035-013-8475-x

Tapia-Abellán, A., Angosto-Bazarra, D., Martínez-Banaclocha, H., de Torre-Minguela, C., Cerón-Carrasco, J.P., Pérez-Sánchez, H., Arostegui, J.I., Pelegrin, P., 2019. MCC950 closes the active conformation of NLRP3 to an inactive state. Nat. Chem. Biol. 15, 560–564. https://doi.org/10.1038/s41589-019-0278-6

Vandanmagsar, B., Youm, Y.H., Ravussin, A., Galgani, J.E., Stadler, K., Mynatt, R.L., Ravussin, E., Stephens, J.M., Dixit, V.D., 2011. The NLRP3 inflammasome instigates obesity-induced inflammation and insulin resistance. Nat. Med. 17, 179–189. https://doi.org/10.1038/nm.2279

Ward, R., Li, W., Abdul, Y., Jackson, L.D., Dong, G., Jamil, S., Filosa, J., Fagan, S.C., Ergul, A., 2019. NLRP3 inflammasome inhibition with MCC950 improves diabetes-mediated cognitive impairment and vasoneuronal remodeling after ischemia. Pharmacol. Res. 142, 237–250. https://doi.org/10.1016/j.phrs.2019.01.035

Yarchoan, M., Toledo, J.B., Lee, E.B., Arvanitakis, Z., Kazi, H., Han, L.-Y., Louneva, N., Lee, V.M.Y., Kim, S.F., Trojanowski, J.Q., Arnold, S.E., 2014. Abnormal serine phosphorylation of insulin receptor substrate 1 is associated with tau pathology in Alzheimer's disease and tauopathies. Acta Neuropathol. 128, 679–689. https://doi.org/10.1007/s00401-014-1328-5

Yekollu, S.K., Thomas, R., O'Sullivan, B., 2011. Targeting curcusomes to inflammatory dendritic cells inhibits NF-κB and improves insulin resistance in obese mice. Diabetes 60, 2928–2938. https://doi.org/10.2337/db11-0275

Yuan, M., Konstantopoulos, N., Lee, J., Hansen, L., Li, Z.W., Karin, M., Shoelson, S.E., 2001. Reversal of obesity- and diet-induced insulin resistance with salicylates or targeted disruption of Ikkβ. Science (80-.). 293, 1673–1677. https://doi.org/10.1126/science.1061620

Zhai, Y., Meng, X., Ye, T., Xie, W., Sun, G., Sun, X., 2018. Inhibiting the NLRP3 Inflammasome Activation with MCC950 Ameliorates Diabetic Encephalopathy in db/db Mice. Molecules 23, 522. https://doi.org/10.3390/molecules23030522

Zhang, J., Wu, W., Li, D., Guo, Y., Ding, H., 2010. Overactivation of NF-κB impairs insulin sensitivity and mediates palmitate-induced insulin resistance in C2C12 skeletal muscle cells. Endocrine 37, 157–166. https://doi.org/10.1007/s12020-009-9283-y

Figure 1

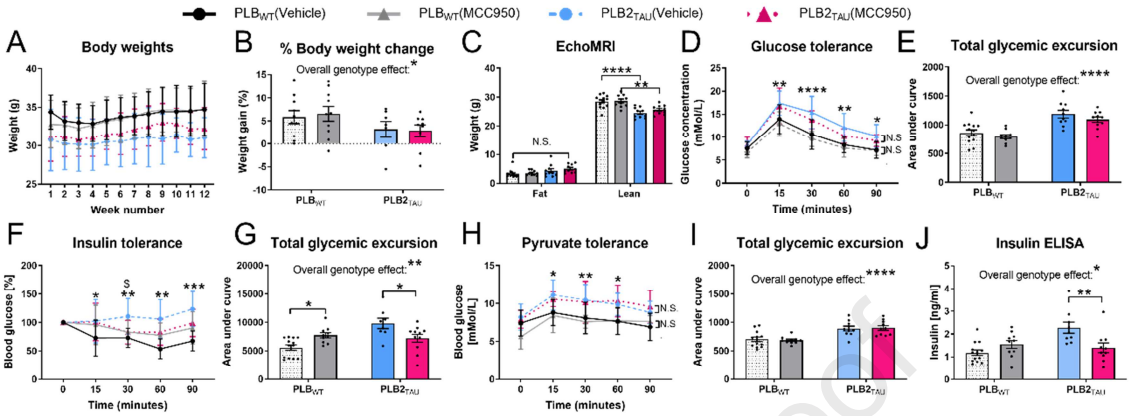

Figure 2

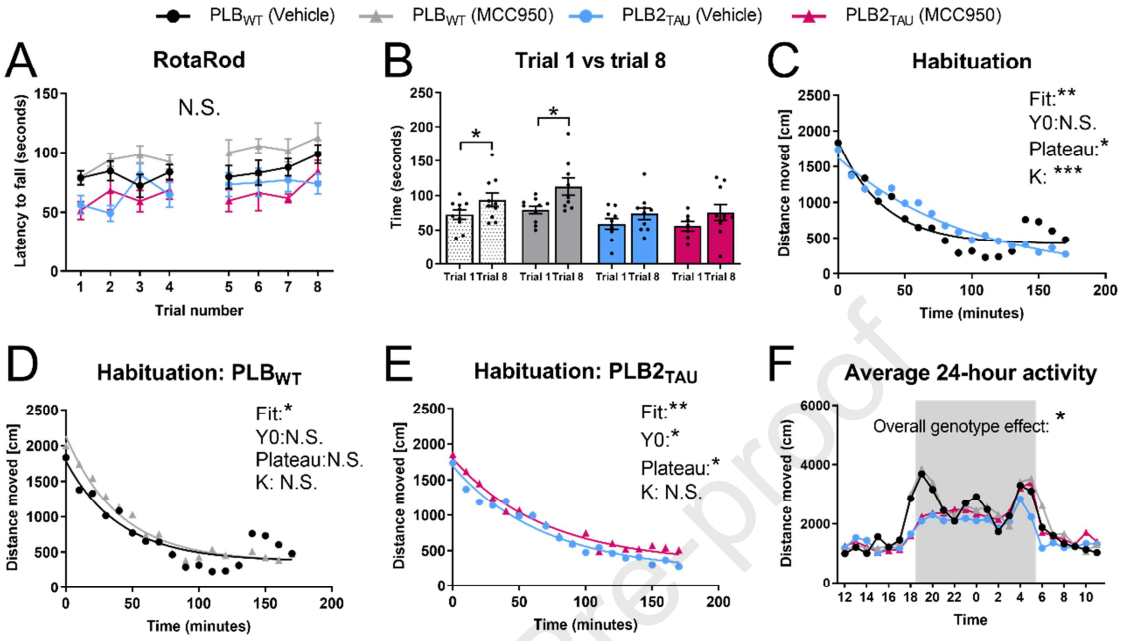

Figure 3

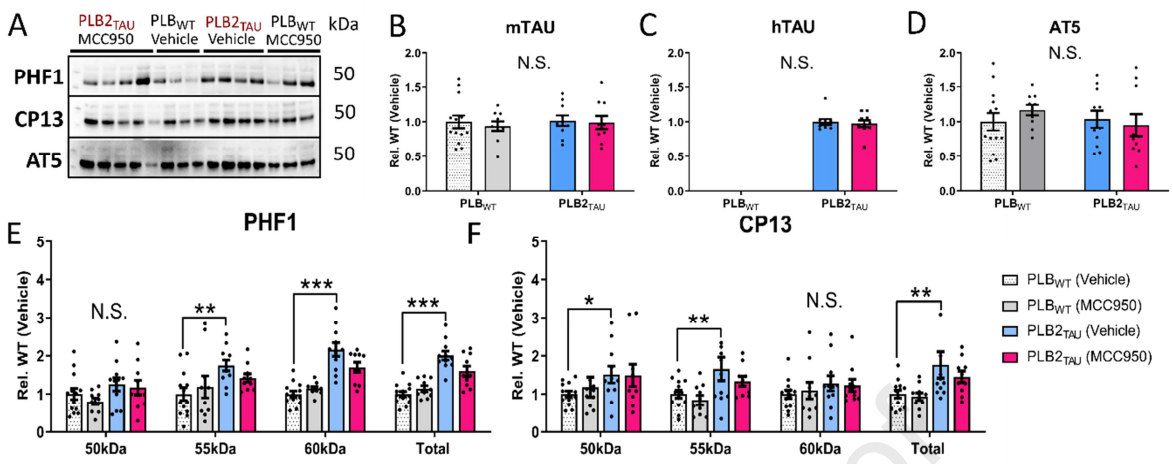

Figure 4

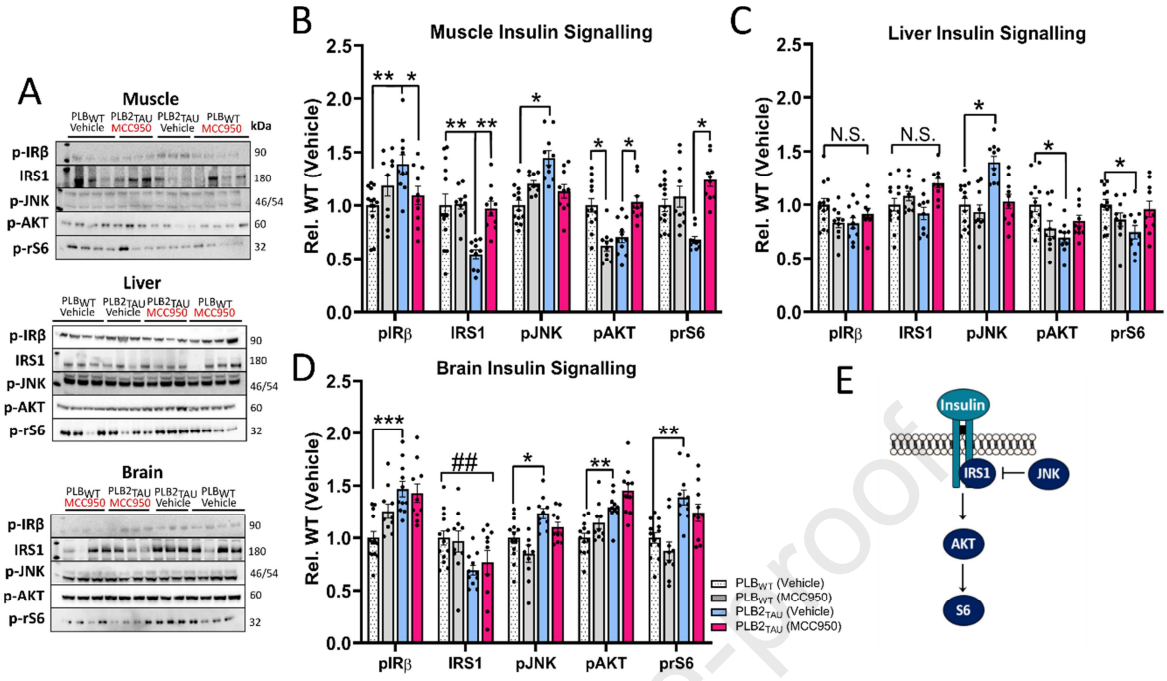

Figure 5

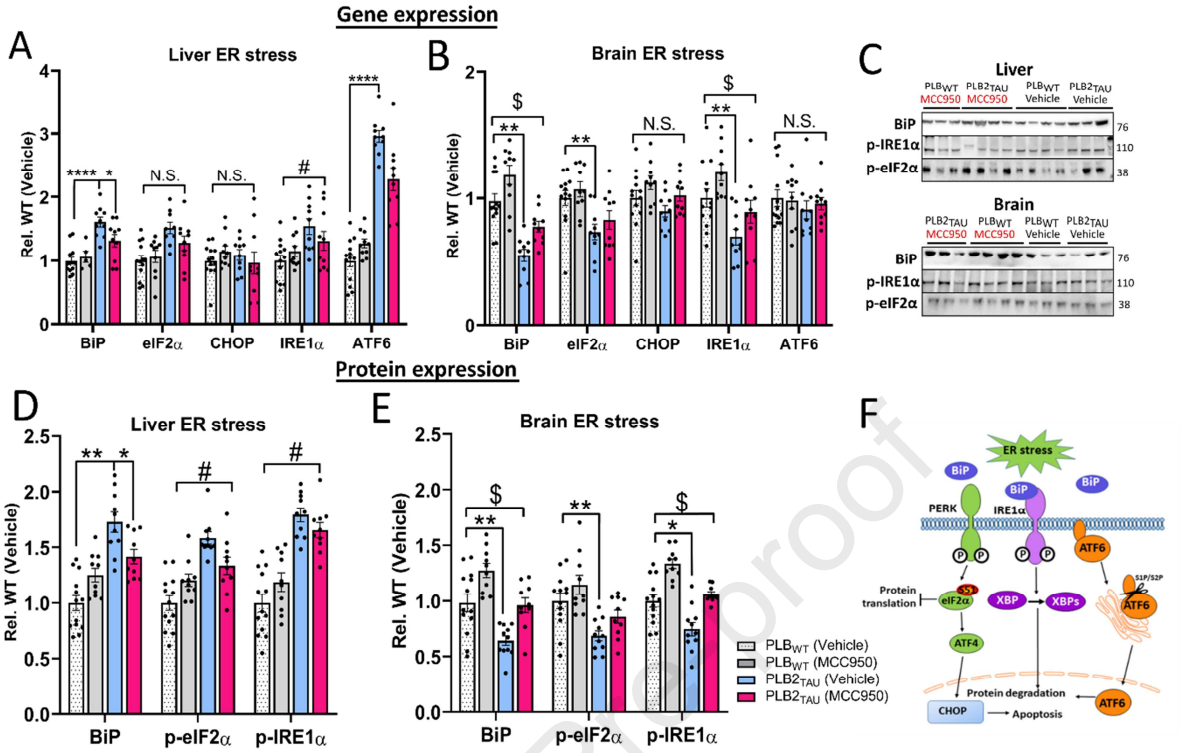

Figure 6

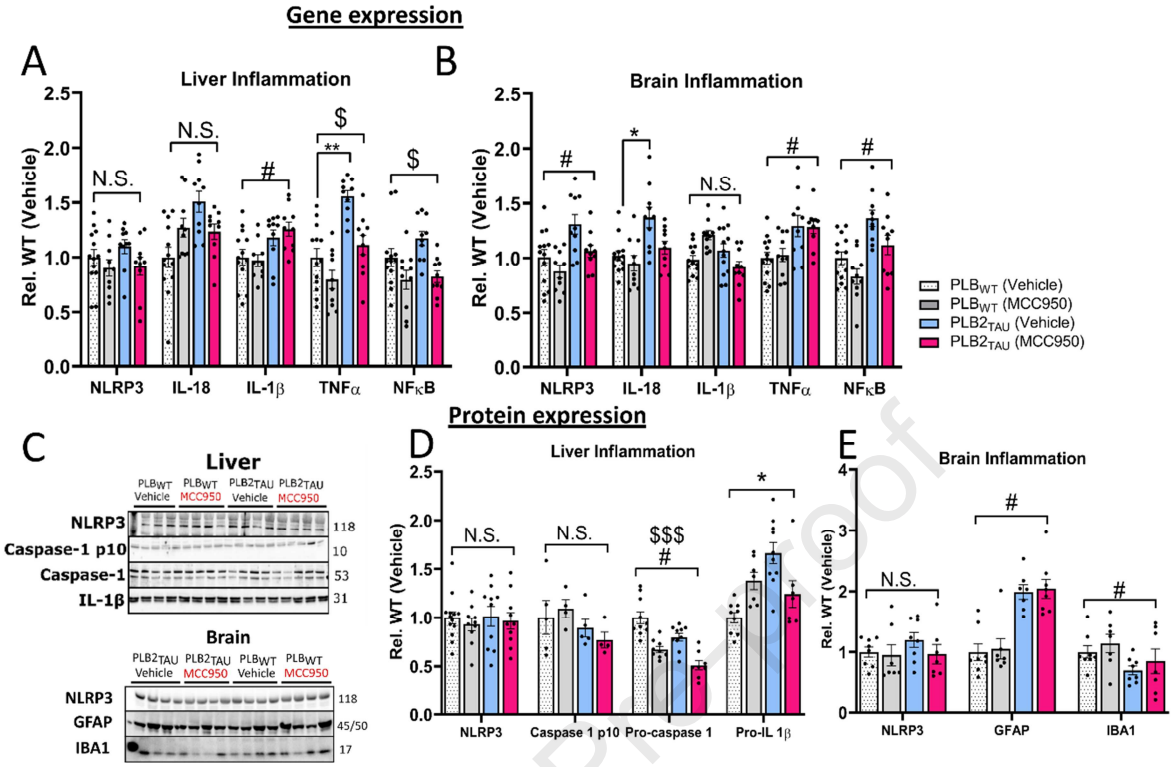

Highlights

- The metabolic role of NLRP3 was investigated in a murine tauopathy model, $PLB2_{Tau}$.
- The inhibitor MCC950 improved glucose tolerance and insulin signalling.
- Inflammation and ER stress was ameliorated in brain and liver.
- In the brain, a partial normalisation of phospho-tau levels was detected.
- MCC950 partially recovered metabolic, inflammatory and FTD-relevant phenotypes.